Extreme chemical variation in complex diamonds from George Creek, Colorado: a SIMS study of carbon isotope composition and nitrogen abundance

I. C. W. Fitzsimons[1,*], B. Harte[1], I. L. Chinn[2], J. J. Gurney[2] and W. R. Taylor[3]

[1] Department of Geology and Geophysics, The University of Edinburgh, The Grant Institute, West Mains Road, Edinburgh EH9 3JW, UK
[2] Department of Geological Sciences, University of Cape Town, Rondebosch 7700, South Africa
[3] Research School of Earth Sciences, Australian National University, Canberra, ACT 0200, Australia

The photographic plate is located in the colour plates section before this papaer.

ABSTRACT

Diamonds from George Creek, Colorado, preserve complex intergrowth textures between two major growth generations: homogeneous diamond with yellow-buff cathodoluminescence (CL); and diamond with blue-green CL and local growth zonation. Secondary-ion mass spectrometry (SIMS) has revealed large variations in N concentration and C isotope composition within these diamonds. Even within single stones, N contents and $\delta^{13}C$ values can vary from 0 to 750 ppm and 0 to $-20‰$ respectively. These variations are similar to those recorded elsewhere for entire diamond suites. The CL characteristics correlate directly with N: diamond with yellow-buff CL has uniform N contents, whereas the zoned diamond has bright blue CL bands with high N (50–750 ppm) and dark blue or green CL bands with low N (0–20 ppm). These bands are too narrow (10–5 µm) for analysis by IR spectroscopy. $\delta^{13}C$ also varies between the two growth generations in any one diamond plate, and to a lesser extent within these generations, but shows no consistent correlations with either CL or N. The George Creek stones preserve evidence of extreme temporal and/or spatial variations in both $\delta^{13}C$ and N concentrations during the period of diamond growth, but the factors controlling N content during diamond growth did not control $\delta^{13}C$.

KEYWORDS: carbon isotopes, cathodoluminescence, diamond, nitrogen concentration, SIMS.

Introduction

NITROGEN is the major impurity in natural diamond, and large variations in N concentration and aggregation state are used to classify natural stones into a number of diamond types (e.g. Harris, 1987). Diamonds also preserve a wide range of C and N isotopic compositions (Deines, 1980; Kirkley *et al.*, 1991; Boyd and Pillinger, 1994; van Heerden *et al.*, 1995), and these isotopic variations are explained in terms of fractionation processes during diamond precipitation in the mantle, or inheritance from a heterogeneous source that possibly includes a component of subducted crustal material (Deines, 1980; Deines *et al.*, 1984, 1987, 1989, 1991; Galimov, 1991; Boyd *et al.*, 1987, 1992, 1994; Boyd and Pillinger, 1994). Stable isotope studies on diamonds generally involve bulk analyses of natural stones, but conventional combustion and gas-source mass spectrometry of diamond fragments or laser-cut sections has shown that significant isotopic variation can also exist within single stones (Swart *et al.*, 1983; Javoy *et al.*, 1984; Galimov, 1991; Boyd *et al.*, 1987, 1994). This is most apparent in coated stones

* Present address: School of Applied Geology, Curtin University of Technology, GPO Box U1987, Perth, WA 6845, Australia

comprising an early diamond core overgrown by a fibrous coat of distinct isotopic composition. Isotopic variation has also been identified within single octahedral stones, but the scale of sectioning for the combustion technique (each fragment has typical dimensions of ~0.5 mm) means that little is known about the detail of this compositional variation, or of any variations associated with the fine-scale growth zonation commonly revealed in natural diamond by cathodoluminescence (CL).

Better knowledge of any zonation patterns in single stones could help resolve the origin or origins of the wide range of diamond composition, and thereby provide information on mantle fluids and diamond growth processes (e.g. Bulanova, 1995). For this reason we have used secondary ion mass spectrometry (SIMS) to map the spatial variation in C isotope composition and N abundance in a number of natural stones. We did not measure N isotope composition as the relatively low total N content in diamond, and hence very low ^{15}N content, coupled with the small sample volume used in SIMS, would result in large uncertainties in the measured isotope ratios relative to the natural isotopic variations. In a companion paper we discuss three diamonds from the Kaapvaal Craton Province of South Africa (Harte et al., 1999), but here we describe the results obtained for three stones from the Colorado-Wyoming Kimberlite Province, USA. These latter stones were chosen for analysis because, in addition to normal growth zonation, they have complex intergrowths between two very distinct diamond growth generations (Chinn, 1995).

The George Creek diamonds

The George Creek kimberlites are part of the State-Line district of the Colorado-Wyoming Kimberlite Province, U.S.A. (Fig. 1). Unlike most diamondiferous kimberlites, which are found within Archaean cratons, the diamond-bearing Colorado-Wyoming Kimberlite Province occurs off craton in a Proterozoic mobile belt accreted onto the southern edge of the Archaean Wyoming Province between 1.8 and 1.6 Ga (Bennett and DePaolo, 1987; Karlstrom and Houston, 1984). These Proterozoic rocks had, however, been thrust northwards over the Wyoming Province before kimberlite emplacement, and it is thought that the kimberlites passed through and sampled Archaean lithosphere before

rising through the Proterozoic rocks exposed at the present-day erosion surface (Eggler et al., 1988; Helmstaedt and Gurney, 1995). Seismic and heat flow data indicate that this Archaean lithospheric keel is no longer present at the southern margin of the Archaean craton (Eggler et al., 1988; Hoffman, 1990), and was probably removed sometime after the end of the Devonian (Eggler et al., 1988; Helmstaedt and Gurney, 1995), which is the age of emplacement for many of the Colorado-Wyoming kimberlites.

The diamonds discussed here (photograhic Plate 3) are part of a large sample of stones collected from the largest of the George Creek kimberlite dykes and studied by Chinn (1995). These stones have a wide range of sizes and morphologies, and their cathodoluminescence (CL) properties were used by Chinn (1995) to distinguish two diamond generations: (1) apparently homogeneous diamond with anomalous yellow-buff or pink CL; and (2) diamond with blue-green CL, which either preserves complex growth zonation or is transected by closely-spaced yellow-green slip planes indicative of high-temperature plastic deformation during mantle residence.

Some stones consist totally of one or other diamond generation (photograhic Plate 3c), but others comprise both generations with complex intergrowth relationships between the two (photograhic Plate 3a, b). We refer to these two generations here as yellow-buff and blue-green diamond, even though these characteristic colours are only visible under cathodoluminescence.

Most mineral inclusions recovered from the George Creek diamonds are of eclogitic paragenesis, and no peridotitic inclusions have been identified (Chinn, 1995). The only inclusions unequivocally associated with yellow-buff diamond are graphite rosettes, rutile and a single inclusion of coesite. In contrast, blue-green diamond contains various inclusion combinations, including several examples of garnet−clinopyroxene (both touching and non-touching) and two examples of orthopyroxene−clinopyroxene (always touching and assumed to be of websteritic paragenesis). Non-touching garnet−clinopyroxene pairs yield temperature estimates of 1078−1178°C (with a mean value of 1138°C) using the Ellis and Green (1979) Fe−Mg exchange thermometer at a reference pressure of 50 kbar (Chinn, 1995). Touching garnet−clinopyroxene and clinopyroxene−orthopyroxene inclusions both yielded temperatures of
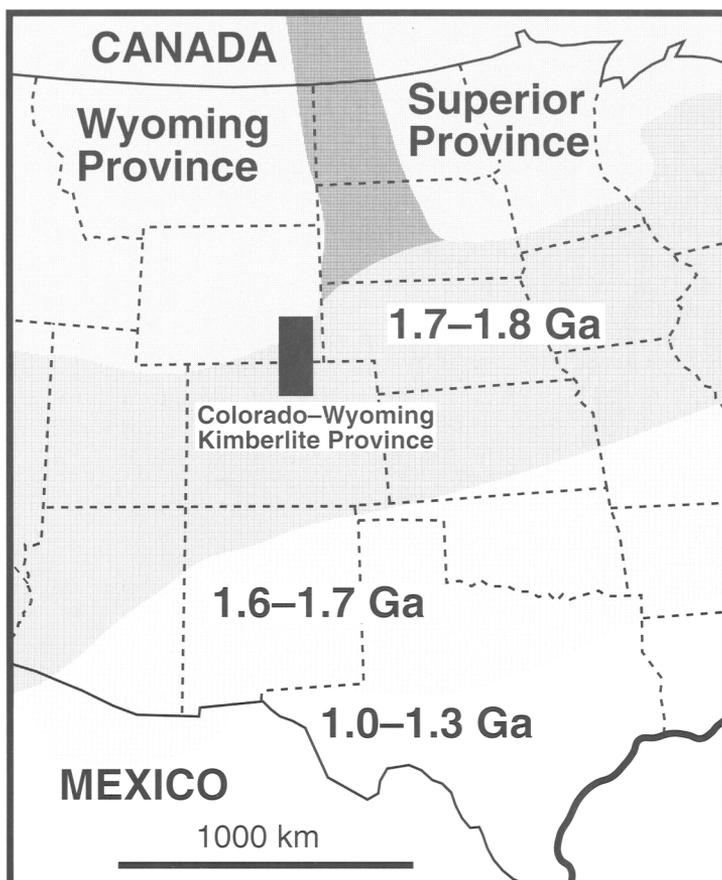
FIG. 1. Geological setting of the Colorado-Wyoming Kimberlite Province (filled box). The Superior and Wyoming Provinces are Archaean cratonic blocks, separated by the Trans Hudson Orogen (dark shading). Basement rocks to the south of these Archaean cratons comprise progressively younger material accreted onto the edge of the craton during the Proterozoic, which are divided into three provinces based on crystallization ages inferred from Nd isotopes (after Reed *et al.*, 1993). The Colorado-Wyoming kimberlites were emplaced into these Proterozoic rocks, but are thought to have passed through underlying Archaean lithosphere (Eggler *et al.*, 1988).

$900-1000°C$ using the Ellis and Green (1979) and Bertrand and Mercier (1985) calibrations respectively. If it is assumed that the two orthopyroxene inclusions were originally in equilibrium with garnet, then the Nickel and Green (1985) barometer gives pressure estimates of 52 and 56 kbar at a reference temperature of 1138°C (Chinn, 1995).

A large number of IR spectra have been gathered on a wide sample of George Creek diamonds (Chinn, 1995), and these indicate that the homogeneous yellow-buff diamond is associated with sub-microscopic CO_2 inclusions, whereas the blue-green diamond has no spectral evidence of CO_2. Total N determinations by IR spectrometry yield very low values for the yellow-buff diamond, which are difficult to quantify, but IR spectra for the blue-green diamond indicate a range of N contents from <40 ppm (the detection limit of the spectrometer) to 2500 ppm. On the basis of the SIMS data reported below, we believe that this wide compositional range is a result of the IR technique sampling diverse growth zones in the blue-green diamond.

Chinn (1995) also used the IR spectra to measure the aggregation state of N in the blue-

green diamond, which is a useful monitor of thermal history. With increased time and/or temperature, N tends to become more aggregated (Evans, 1992); a process involving the migration and combination of single N defects to form pairs (A aggregates) and then groups of four N atoms associated with a vacancy (B aggregates). Aggregation state also depends on N concentration, since the higher the N content, the more likely it is that N will aggregate for a given temperature-time history. Both aggregate types have characteristic IR spectra, and their formation has been calibrated as a function of temperature, time and N concentration (Evans and Harris, 1989; Taylor *et al.*, 1990, 1996). Typically 60–100% of N in the blue-green diamond is present as B type aggregates, which corresponds to an equilibration temperature of ~1220°C given the measured N contents and an assumed mantle residence time of 1.25 Ga (Chinn, 1995). This residence time is a very approximate estimate, based on the ages of diamonds from elsewhere, but choosing a different time (e.g. 1.0 Ga or 3.0 Ga) has limited effect on the temperature calculations as the aggregation state is much more dependent on temperature than time. The apparent 100°C discrepancy between the temperature based on N aggregation and temperature estimates from inclusion thermobarometry was attributed by Chinn (1995) to deformation-enhanced N aggregation, although other possibilities include a large underestimate of the mantle residence time, a heating event subsequent to diamond formation that is not recorded by the mineral inclusions, or uncertainty in the kinetics of the aggregation process. Another factor, considered further below, is that small-scale (<50 μm) variations in N content cannot be resolved by the IR technique. This means that high aggregation states might reflect high concentrations of N within particular growth zones, even though the overall N content of the diamond measured by IR spectroscopy is low.

The relative ages of the two diamond growth episodes is unclear, and the lack of N defects or suitable mineral inclusions in the yellow-buff diamond precludes any comparison of the thermal history of this diamond generation with that of the blue-green diamond. Stones comprising both growth generations generally have a central core of homogeneous yellow-buff diamond with outer zones of blue-green diamond. The contact between the two is typically irregular in shape (photograhic Plate 3*a*, *b*), and growth zones in the outer blue-green diamond commonly mimic the shape of this contact, suggesting that the yellow-buff core is older than the blue-green diamond. However, intergrowth textures in some stones suggest that the yellow-buff diamond has filled fractures in the blue-green diamond, and a similar sequence of diamond growth is implied by those stones in which apparently undeformed yellow-buff diamond coexists with intensely deformed blue-green diamond (Chinn, 1995). Another possibility is that there is more than one generation of blue-green diamond.

Sample description

Plates cut from three of the George Creek stones were selected for SIMS analysis; GC008, GC030 and GC042 (Chinn, 1995). These diamond plates preserve a number of interesting CL features described by Chinn (1995). Each of the plates has two parallel polished surfaces, and for plates GC008 and GC030 we have analysed the same surfaces described and illustrated by Chinn (1995). We analysed the reverse face of plate GC042, but in all three cases our data are comparable with the IR N analyses of Chinn (1995), since the latter is a transmission technique that sampled the entire thickness of the diamond plate.

Plate GC008

This large plate (~5 mm × 4 mm and 0.5 mm thick; photograhic Plate 3*a*) is dominated by a central region with buff CL, associated with CO_2-bearing inclusions in the diamond lattice. This area appears generally homogeneous, although local patterns do occur and Chinn (1995) suggested that these may reflect the annealing of fluid inclusions. Areas of CO_2-free diamond with blue-green CL occur at the edges of the anomalous central zone. These outer zones are dominated by green CL with numerous closely spaced yellow-green slip planes, but a number of narrow bright blue CL zones occur both within the green zones and at their contact with the central buff diamond. The N content of this plate was below the detection limit of the IR spectrometer (Chinn, 1995).

Plate GC030

This plate (~4 mm × 2 mm and 1.6 mm thick; Plate 3*b*) is another composite stone with two zones of quite distinct CL. A relatively homo-

geneous central region with yellow CL has spectral evidence of CO_2 inclusions. Areas with complex banding of green, dark blue and bright blue CL occur at the edges of the plate, and correlate with CO_2-free parts of the stone. A small area of diamond with yellow CL also occurs at the edge of the stone, and is separated from the central homogeneous yellow zone (at least on the plate surface) by diamond with blue-green banded CL. Unlike many of the other George Creek stones, the blue-green diamond in this plate has little evidence of plastic deformation and the complex banding in this diamond is presumably an original growth feature. The IR spectra (Chinn, 1995) indicate relatively low N contents in the blue-green diamond (100 to 130 ppm) with a relatively high degree of N aggregation (75 to 85% of N present as B defects). Any N present in the homogeneous yellow diamond was below the detection limit of the IR spectrometer.

Plate GC042

Unlike the other two plates discussed here, plate GC042 (~3 mm × 2 mm and 1.6 mm thick; photograhic Plate 3c) is not a composite stone and consists only of CO_2-free diamond. It is dominated by diffuse zones of bright blue and green CL dissected by three orientations of yellow slip plane intersecting at 60° on the plate surface. In general it is difficult to identify any definite pattern in the distribution of bright blue and green CL zones, although bright blue CL zones do occur as distinct planar growth zones on the side of the plate that we did not analyse. Infrared spectra obtained from this plate indicate N contents of 26−172 ppm, with 56−82% of the N in each spectrum present as B-type defects (Chinn, 1995).

Analytical technique

The natural diamond plates and two polished fragments of a synthetic diamond standard were mounted in indium within an aluminium sample mount, and pressed to give a flat surface. Details of the standard material (synthetic A: N content = 230.4 ppm; $\delta^{13}C$ = −23.924‰) are given by Harte et al. (1999). The sample mount was washed with acetone in an ultrasonic bath, and coated with a thin layer of gold (~0.02 µm). Lines of silver DAG were painted on the surface to connect the edges of the natural and synthetic diamonds with the sample holder. N abundance and C isotope composition were measured using

the CAMECA ims-4f ion microprobe (Slodzian, 1980) with a Charles Evans and Associates control system at the Department of Geology and Geophysics, University of Edinburgh. The data reported here were collected in several analytical sessions during March and August 1995, using analytical techniques similar to those described by Harte and Otter (1992) and Harte et al. (1999). In the case of both N and C analyses, it appears that diamond is sufficiently conductive to dissipate any charge build-up at the sample surface, and the charge neutralization techniques employed for SIMS analysis of minerals like quartz were not needed.

Technique for N analysis

Nitrogen does not readily form N^+ or N^- ions, and SIMS studies generally use the NC^-/C^- ratio as a relative measure of N abundance (Zinner et al., 1989). We analysed secondary $^{14}N^{12}C^-$ and $^{13}C^-$ ions from the diamond samples and the standard of known N content using a focused Cs^+ primary beam (diameter ~20 µm, current = 7 to 8 nA). The primary beam was accelerated at a potential of +10 kV onto the sample, and the sputtered secondary ions were accelerated at a potential of −4.5 kV towards the electrostatic energy filter and mass analyser, via a series of apertures which ensured that only the central 8 µm of the sputtered area was analysed. Analyses were performed at high mass resolution (m/Δm $\approx$ 7500) so as to distinguish $^{14}N^{12}C^-$ from $^{13}C_2^-$, which is the principal interference. The level of adsorbed N on the sample surface was limited by operating at high vacuum in the sample chamber.

Technique for C isotope analysis

Carbon isotopes were analysed by sputtering the sample with a primary beam of $^{133}Cs^+$ and using the relative yields of secondary $^{12}C^-$ and $^{13}C^-$ ions to determine the isotope composition by comparison with yields from the standard of known $\delta^{13}C$. As for N analysis, the primary beam was accelerated at a potential of +10 kV onto the sample. The principal molecular interference is that between $^{13}C^-$ and $^{12}CH^-$ ions, and this was dealt with in two ways. The analyses of March 1995 were carried out at low mass resolution using a 300 V energy offset, such that the sputtered secondary ions were accelerated at a potential of −4.2 kV towards the electrostatic energy filter and mass analyser (rather than the

usual potential of -4.5 kV). This means that only those ions that leave the sample with a high kinetic energy are selected for analysis, which suppresses $^{12}CH^-$ in the secondary ion beam. However, the analyses carried out in August 1995 used a high mass resolution (m/Δm $\approx$ 4300) to separate $^{13}C^-$ and $^{12}CH^-$ ions, and in this case the secondary ions were accelerated away from the sample at the usual potential of -4.5 kV. The degree of hydride interference was also minimized in both cases by maintaining a high vacuum in the sample chamber ($< 2 \times 10^{-9}$ Torr). The March analyses used a defocused primary beam (20−30 μm pit diameter on the sample) with a beam current of ~5 nA, but the August session used a smaller primary beam (~8 μm) with a beam current of ~0.5 nA.

Analytical procedure

Nitrogen and C analyses followed a similar procedure. After a 5 min burn-in time to remove the gold coat and allow the sputtering process to achieve a steady state, the negative secondary beam was analysed using an ETP AF133 electron multiplier. Each N analysis comprised 50 measurement pairs, each with one counting period for ^{13}C (2 s) and one for $^{14}N^{12}C$ (2 s). Each C isotope analysis comprised 100 measurement pairs, each with one counting period for ^{12}C (1 s) and one for ^{13}C (5 s). The magnetic peak switching from one mass to the other was controlled by the Charles Evans and Associates computer system. The primary beam current was checked before and after each analysis and adjusted if there was significant drift. The position of the primary ion beam with respect to the secondary ion optics was also checked before the start of each analysis and adjusted, if necessary, by moving the primary beam position. In addition, the magnet was re-calibrated during the burn-in time at the start of each analysis.

Analysis points on the sample were typically arranged in linear transects across the various CL zones in each plate, and the synthetic standards were analysed at regular time intervals, typically after every 3−5 sample analyses. The points in each transect were analysed in a random order, rather than consecutively from one end to the other, so that any patterns in the data are likely to represent real compositional variation rather than instrumental changes with time. The exact location of the analysis points with respect to the various CL zones in each plate was determined from CL photographs of the plates taken after each analytical session.

Analytical results

The count data for sample and standard analyses were expressed in terms of $^{14}N^{12}C/^{13}C$ or $^{13}C/^{12}C$ ratios for each pair of measurements. These were corrected for the counting system dead time and any obvious outliers removed, and the remaining data were used to calculate a mean value of $^{14}N^{12}C/^{13}C$ or $^{13}C/^{12}C$ for each analysis point. Mean values of $^{14}N^{12}C/^{13}C$ and $^{13}C/^{12}C$ for all the N and C analyses of the standard are plotted as a function of time in Figs 2 and 3.

Regression lines for the standard N data (Fig. 2) indicate that there was negligible analytical drift with time, and that major analytical breaks have little effect on measured ion ratios. The $^{14}N^{12}C/^{13}C$ ratios for the individual analysis points do show a wide spread around the regression lines, which is significantly larger than the analytical uncertainty. This could reflect a heterogeneity in the N content of the synthetic diamond standard (Harte et al., 1999), but these variations are negligible compared with the wide range of $^{14}N^{12}C/^{13}C$ ratios measured in the natural diamond plates, and do not affect the suitability of the synthetic diamond as a N standard in this study.

In contrast, the C data are particularly sensitive to changes in the instrumental set up (Fig. 3), and even under relatively stable conditions there is commonly a progressive drift of $^{13}C/^{12}C$ ratios measured in the standard with time. This variation has been modelled by least-squares regression (Fig. 3), and the spread of individual analysis points about the regression lines is similar to that expected from the analytical uncertainty, indicating that the standard is homogeneous with respect to C isotopes (see Fitzsimons et al., in press, for further details). Other SIMS studies at Edinburgh have identified a similar drift in isotope ratio, typically with the relative number of counts of the heavy isotope decreasing relative to the light isotope (e.g. Valley and Graham, 1991; Harte and Otter, 1992; Eiler et al., 1995; Smith and Yardley, 1996) and it has been suggested that this reflects progressive ageing of the electron multiplier (Eiler et al., 1995). Drift in the reverse sense is also observed (Fig. 3c), typically immediately after instrument start up or major realignment, and presumably represents an instrumental response to changes in the primary and/or secondary column.
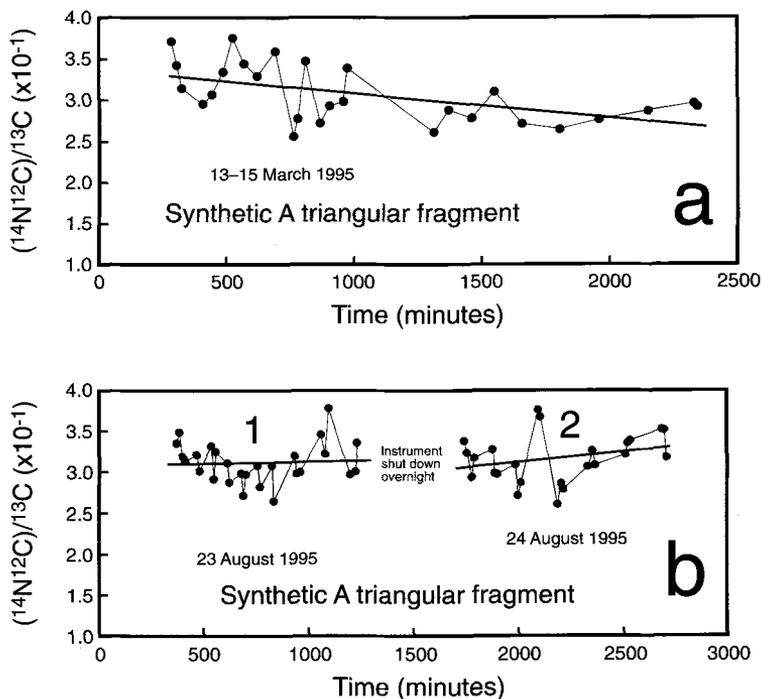
FIG. 2. $^{14}N^{12}C^-/^{13}C^-$ ion ratios for all of the N analyses made on the synthetic diamond standard during March and August 1995. Each point represents the mean ratio for a single analysis point, comprising 50 repeated ratio measurements, and the data have been corrected for the dead-time of the counting system. The ± 1 s analytical uncertainty in the $^{14}N^{12}C^-/^{13}C^-$ ratio for each analysis point is smaller than the symbol size in the figure $(0.005 \times 10^{-1} <1$ s $<0.05 \times 10^{-1})$. Each analysis lasted ~15 min, and the time shown in this Figure represents the start of each analysis, measured in minutes from the beginning of the analytical session. These standard analyses were interspersed with analyses of the natural diamond plates. Least-squares regression lines are shown for these standard data, and were used to calibrate the sample analyses (Fitzsimons et al., in press).

Mean values of $^{14}N^{12}C/^{13}C$ or $^{13}C/^{12}C$ for each analysis point on the natural diamond plates are listed in Table 1, which also gives the corresponding N concentrations or $\delta^{13}C$ values calculated by calibration against the standard regression lines in Figs 2 and 3 (see Fitzsimons et al., in press, for a discussion of the calibration procedure). Analyses are presented in chronological order and are divided into separate sessions on the basis of the corresponding standard calibration line. Figures 5, 6 and 7 illustrate these data in terms of analytical transects across each plate, and Figs 8 and 9 present the same data as histograms to emphasise the compositional differences both within and between plates. Uncertainties in the measured ion ratios (Figs 2, 3 and Table 1) and in the calculated values of N concentration or $\delta^{13}C$ (Figs 5, 6, 7

and Table 1) are all in terms of ± 1 s (rather than ± 2 s). Typical analytical uncertainties in the final calculated values of N concentration and $\delta^{13}C$ are ± 2 to 5% and ± 0.6 to 1.2‰ respectively (see Fitzsimons et al., in press, for a discussion of precision in SIMS stable isotope analysis).

Plate GC008

Nitrogen and C analyses of this plate were made along four transects (Fig. 4) and the data for these transects are summarized in Fig. 5. The central buff CL zone has N contents of 25–75 ppm, whereas the outer blue-green zones generally have very low N contents of 0–20 ppm. However, the bright blue CL bands within and at the edges of these outer zones have distinctly
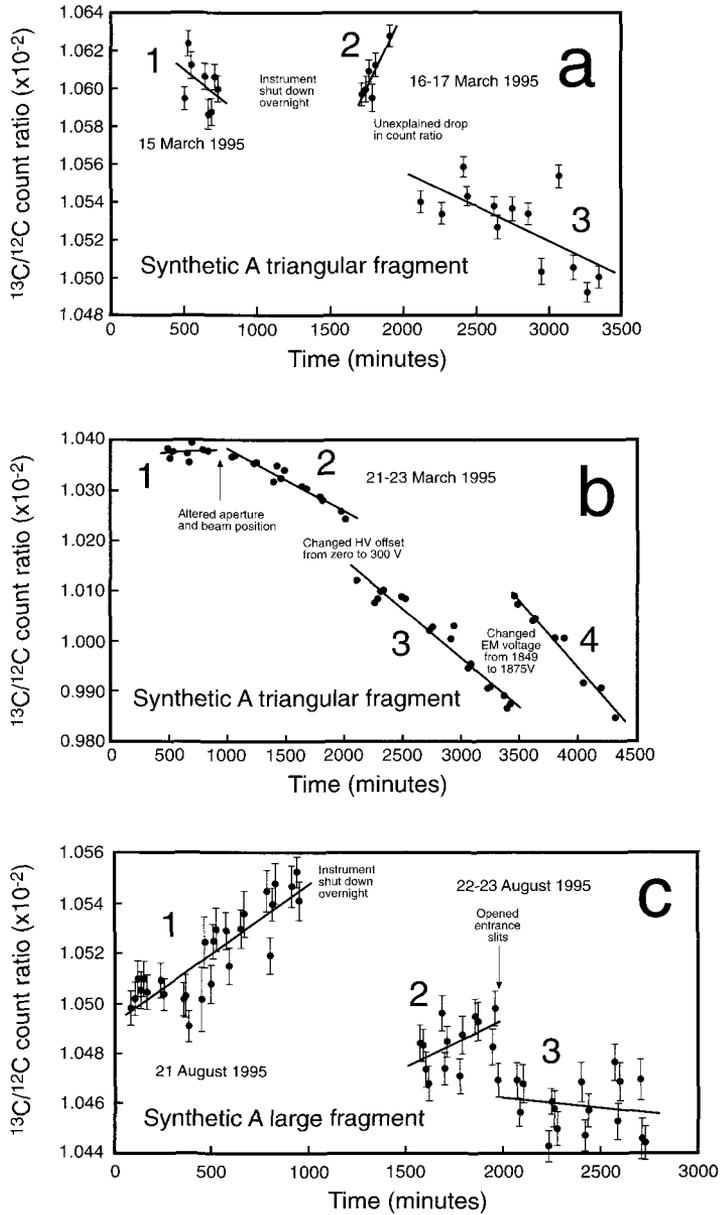
FIG. 3. $^{13}C^-/^{12}C^-$ ion ratios for all C analyses made on the synthetic diamond standard during March and August 1995. Each point represents the mean ratio for a single analysis point, comprising 100 repeated ratio measurements, and the data have been corrected for the dead-time of the counting system. Error bars represent ± 1 s analytical uncertainty, and are not shown in b as they are about the same size as the symbols (the uncertainty in b is actually of similar magnitude to that in a and c, but the scale of the count-ratio axis is different). Each analysis lasted about 20 min, and the time shown in this figure represents the start of each analysis, measured in minutes, from the beginning of the analytical session. These standard analyses were interspersed with analyses of the natural diamond plates. Least-squares regression lines are shown for these standard data, and were used to calibrate the sample analyses (Fitzsimons et al., in press).
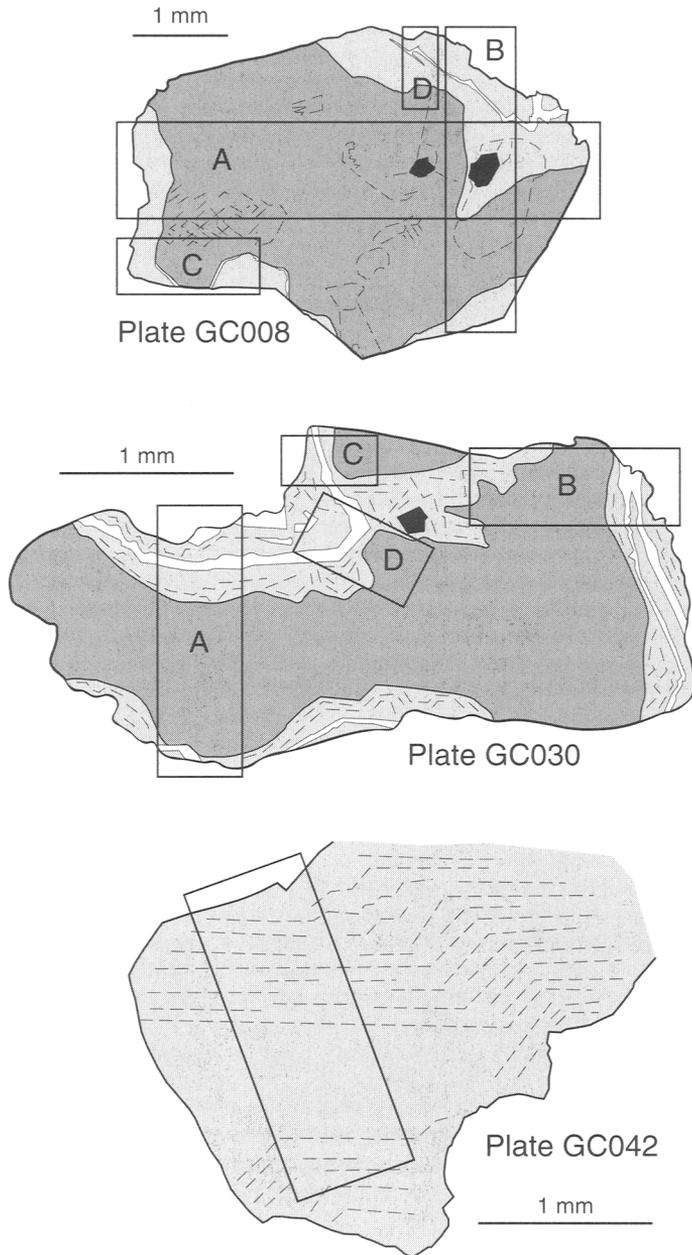
FIG. 4. Schematic representations of the CL photographs in photografhic Plate 3a (GC008), 3b (GC030) and 3c (GC042). Dark grey areas are diamond with homogeneous yellow-buff CL and light grey represents diamond with blue-green CL. White bands indicate prominent bright blue CL zones within and at the edges of the blue-green CL zones, and black areas are mineral inclusions. Deformation and cracks near inclusions at the right side of GC008 make it impossible to represent all blue-green CL zones in this area, and the deformed and diffuse nature of blue-green CL zones in GC042 mean that no CL boundaries are depicted for this plate. Boxes indicate the locations of analytical transects depicted in detail in Figs 5, 6 and 7.

TABLE 1. Summary of SIMS N and C data for the George Creek plates

N analyses

Analysis label	$^{12}C^{14}N/^{13}C \pm 1$ s ($\times 10^{-4}$)	N content ± 1 s (ppm N)	Analysis label	$^{12}C^{14}N/^{13}C \pm 1$ s ($\times 10^{-4}$)	N content ± 1 s (ppm N)
13–15 March 1995		Standard regression line 2a			
GC030-1	2283 ± 126	177.6 ± 10.5	GC008-3	493 ± 4	40.3 ± 1.4
GC030-2	216 ± 3	16.8 ± 0.4	GC008-4	431 ± 3	35.3 ± 1.2
GC030-3	221 ± 2	17.3 ± 0.4	GC008-5	519 ± 3	42.5 ± 1.5
GC030-4	198 ± 2	15.5 ± 0.4	GC008-6	693 ± 7	56.9 ± 2.0
GC030-5	257 ± 2	20.2 ± 0.5	GC008-7	647 ± 6	53.2 ± 1.9
GC030-6	236 ± 2	18.6 ± 0.5	GC008-8	427 ± 2	35.4 ± 1.3
GC030-7	234 ± 2	18.4 ± 0.5	GC008-9	454 ± 4	37.8 ± 1.5
GC030-8	214 ± 1	16.9 ± 0.4	GC008-10	589 ± 9	49.1 ± 2.0
GC030-9	230 ± 2	18.2 ± 0.5	GC008-11	348 ± 4	29.1 ± 1.2
GC030-10	238 ± 2	18.9 ± 0.5	GC008-12	302 ± 2	25.3 ± 1.0
GC030-11	233 ± 3	18.5 ± 0.6	GC008-13	613 ± 10	51.5 ± 2.3
GC030-12	5.82 ± 0.09	0.5 ± 0.0	GC008-14	844 ± 3	71.5 ± 3.1
GC030-13	5773 ± 34	463.9 ± 13.5	GC008-15	664 ± 6	56.4 ± 2.6
GC030-14	278 ± 13	22.4 ± 1.2	GC008-16	1.01 ± 0.04	0.1 ± 0.0
GC030-15	55.3 ± 0.3	4.5 ± 0.1	GC008-17	0.89 ± 0.04	0.1 ± 0.0
GC030-16	5179 ± 25	418.8 ± 12.7	GC008-18	102 ± 0.5	8.7 ± 0.4
GC008-1	1.45 ± 0.04	0.1 ± 0.0	GC008-19	446 ± 6	38.1 ± 1.9
GC008-2	430 ± 4	35.0 ± 1.2	GC008-20	12.1 ± 0.4	1.0 ± 0.1
23 August 1995		Standard regression line 2b1			
GC030-17	3204 ± 112	236.9 ± 9.1	GC008-23	248 ± 3	18.3 ± 0.5
GC030-18	115 ± 3	8.5 ± 0.2	GC008-24	947 ± 16	69.8 ± 1.9
GC030-19	128 ± 3	9.5 ± 0.3	GC008-25	908 ± 3	66.9 ± 1.5
GC030-20	1618 ± 6	119.6 ± 2.0	GC008-26	1080 ± 17	79.5 ± 2.2
GC030-21	4253 ± 48	314.1 ± 6.2	GC008-27	141 ± 4	10.3 ± 0.4
GC030-22	315 ± 2	23.2 ± 0.4	GC008-28	103 ± 2	7.5 ± 0.2
GC030-23	349 ± 3	25.8 ± 0.5	GC008-29	1044 ± 15	76.7 ± 2.4
GC030-24	1719 ± 4	126.9 ± 2.2	GC008-30	78.0 ± 0.6	5.7 ± 0.2
GC030-25	3922 ± 39	289.4 ± 5.9	GC008-31	172 ± 3	12.6 ± 0.4
GC008-21	129 ± 3	9.5 ± 0.3	GC008-32	830 ± 3	61.0 ± 1.8
GC008-22	142 ± 3	10.5 ± 0.3			
24 August 1995		Standard regression line 2b2			
GC030-26	98.6 ± 0.9	7.4 ± 0.2	GC042-11	454 ± 3	33.1 ± 0.6
GC030-27	85.1 ± 1.0	6.4 ± 0.2	GC042-12	103 ± 1	7.5 ± 0.1
GC030-28	72.7 ± 1.0	5.4 ± 0.2	GC042-13	498 ± 2	36.1 ± 0.7
GC030-29	275 ± 2	20.6 ± 0.6	GC042-14	524 ± 7	38.0 ± 0.9
GC030-30	1964 ± 9	146.8 ± 3.8	GC042-15	94.4 ± 1.4	6.8 ± 0.2
GC030-31	212 ± 2	15.8 ± 0.4	GC042-16	939 ± 8	67.9 ± 1.4
GC030-32	253 ± 1	18.8 ± 0.4	GC042-17	2550 ± 29	184.1 ± 4.1
GC030-33	6114 ± 10	454.2 ± 10.4	GC042-18	1075 ± 14	77.6 ± 1.8
GC030-34	207 ± 1	15.4 ± 0.4	GC042-19	487 ± 3	35.1 ± 0.7
GC030-35	216 ± 1	16.0 ± 0.4	GC042-20	521 ± 2	37.5 ± 0.7
GC030-36	220 ± 1	16.3 ± 0.4	GC008-33	748 ± 7	53.5 ± 1.3
GC030-37	137 ± 1	10.1 ± 0.2	GC008-34	260 ± 3	18.5 ± 0.5
GC042-1	394 ± 4	29.0 ± 0.6	GC008-35	177 ± 5	12.6 ± 0.5
GC042-2	288 ± 3	21.2 ± 0.5	GC008-36	146 ± 4	10.4 ± 0.4
GC042-3	230 ± 1	16.9 ± 0.3	GC008-37	771 ± 5	54.9 ± 1.3
GC042-4	386 ± 1	28.3 ± 0.6	GC008-38	640 ± 6	45.5 ± 1.2
GC042-5	1249 ± 9	91.7 ± 1.9	GC008-39	319 ± 3	22.6 ± 0.6
GC042-6	417 ± 2	30.6 ± 0.6	GC008-40	90.8 ± 1.4	6.4 ± 0.2
GC042-7	1356 ± 8	99.1 ± 1.9	GC008-41	895 ± 3	63.2 ± 1.8
GC042-8	380 ± 4	27.8 ± 0.6	GC008-42	1044 ± 11	73.6 ± 2.2
GC042-9	589 ± 2	43.0 ± 0.8	GC008-43	10650 ± 120	749.4 ± 23.7
GC042-10	1826 ± 12	133.1 ± 2.5	GC008-44	1553 ± 29	109.2 ± 3.9

TABLE 1. (*contd.*) C analyses

Analysis label	$^{13}C/^{12}C \pm 1$ s $(\times 10^{-2})$	$\delta^{13}C \pm 1$ s (‰PDB)	Analysis label	$^{13}C/^{12}C \pm 1$ s $(\times 10^{-2})$	$\delta^{13}C \pm 1$ s (‰PDB)
16 March 1995	**Standard regression line 3a2**		Δ initial = −33.19‰	Δ final = −30.43‰	
GC030-1	1.0710 ± 0.0006	−15.16 ± 0.67	GC030-6	1.0655 ± 0.0006	−17.74 ± 1.92
GC030-2	1.0671 ± 0.0006	−19.10 ± 0.69	GC030-7	1.0671 ± 0.0006	−17.21 ± 1.51
GC030-3	1.0693 ± 0.0007	−17.42 ± 0.78	GC030-8	1.0674 ± 0.0006	−17.29 ± 1.36
GC030-4	1.0727 ± 0.0005	−15.45 ± 0.89	GC030-9	1.0672 ± 0.0006	−17.94 ± 1.23
GC030-5	1.0656 ± 0.0006	−17.29 ± 2.11			
16–17 March 1995	**Standard regression line 3a3**		Δ initial = −37.10‰	Δ final = −41.10‰	
GC030-10	1.0732 ± 0.0006	−14.93 ± 1.28	GC008-3	1.0636 ± 0.0006	−13.64 ± 0.72
GC030-11	1.0715 ± 0.0006	−15.93 ± 1.20	GC008-4	1.0673 ± 0.0007	−10.08 ± 0.79
GC030-12	1.0691 ± 0.0007	−17.50 ± 1.16	GC008-5	1.0634 ± 0.0006	−13.60 ± 0.72
GC030-13	1.0676 ± 0.0006	−16.95 ± 0.97	GC008-6	1.0581 ± 0.0006	−18.42 ± 0.76
GC030-14	1.0712 ± 0.0006	−12.95 ± 0.94	GC008-7	1.0605 ± 0.0006	−15.97 ± 0.74
GC030-15	1.0630 ± 0.0006	−15.86 ± 0.82	GC008-8	1.0771 ± 0.0006	−0.46 ± 0.76
GC030-16	1.0673 ± 0.0006	−11.74 ± 0.83	GC008-9	1.0713 ± 0.0006	−5.77 ± 0.81
GC030-17	1.0609 ± 0.0006	−17.23 ± 0.75	GC008-10	1.0757 ± 0.0006	−1.53 ± 0.83
GC030-18	1.0651 ± 0.0007	−13.28 ± 0.78	GC008-11	1.0759 ± 0.0006	−1.29 ± 0.82
GC030-19	1.0614 ± 0.0006	−16.58 ± 0.71	GC008-12	1.0708 ± 0.0006	−5.95 ± 0.84
GC030-20	1.0606 ± 0.0006	−17.25 ± 0.73	GC008-13	1.0610 ± 0.0007	−14.86 ± 0.92
GC030-21	1.0601 ± 0.0006	−17.47 ± 0.69	GC008-14	1.0591 ± 0.0006	−16.54 ± 0.87
GC030-22	1.0633 ± 0.0007	−14.37 ± 0.74	GC008-15	1.0612 ± 0.0006	−14.52 ± 0.90
GC030-23	1.0576 ± 0.0006	−19.63 ± 0.72	GC008-16	1.0588 ± 0.0007	−16.53 ± 1.00
GC008-1	1.0624 ± 0.0006	−14.95 ± 0.69	GC008-17	1.0735 ± 0.0006	−2.77 ± 0.96
GC008-2	1.0644 ± 0.0006	−13.06 ± 0.68			
22 March 1995	**Standard regression line 3b4**		Δ initial = −78.20‰	Δ final = −98.47‰	
GC042-1	1.0145 ± 0.0008	−6.68 ± 0.91	GC042-7	1.0093 ± 0.0008	−6.41 ± 1.05
GC042-2	1.0171 ± 0.0009	−3.46 ± 1.01	GC042-8	1.0099 ± 0.0009	−5.16 ± 1.13
GC042-3	1.0158 ± 0.0008	−4.03 ± 0.96	GC042-9	1.0082 ± 0.0009	−4.76 ± 1.21
GC042-4	1.0126 ± 0.0008	−6.50 ± 0.98	GC042-10	1.0061 ± 0.0008	−6.26 ± 1.18
GC042-5	1.0090 ± 0.0008	−7.91 ± 1.00	GC042-11	1.0104 ± 0.0008	−1.27 ± 1.24
GC042-6	1.0100 ± 0.0007	−6.29 ± 1.02	GC042-12	1.0058 ± 0.0008	−5.16 ± 1.24
21 August 1995	**Standard regression line 3c1**		Δ initial = −41.94‰	Δ final = −37.73‰	
GC030-24	1.0621 ± 0.0007	−16.39 ± 0.78	GC030-26	1.0677 ± 0.0006	−11.29 ± 0.60
GC030-25	1.0655 ± 0.0007	−13.29 ± 0.72	GC030-27	1.0635 ± 0.0006	−15.26 ± 0.67
22 August 1995	**Standard regression line 4c2**		Δ initial = −43.69‰	Δ final = −42.37‰	
GC030-28	1.0563 ± 0.0006	−16.12 ± 0.64	GC030-37	1.0560 ± 0.0007	−17.09 ± 0.67
GC030-29	1.0587 ± 0.0006	−13.93 ± 0.67	GC030-38	1.0568 ± 0.0008	−16.40 ± 0.79
GC030-30	1.0574 ± 0.0007	−15.28 ± 0.73	GC030-39	1.0588 ± 0.0008	−14.62 ± 0.80
GC030-31	1.0547 ± 0.0008	−17.75 ± 0.78	GC030-40	1.0594 ± 0.0008	−14.18 ± 0.83
GC030-32	1.0592 ± 0.0007	−13.78 ± 0.67	GC030-41	1.0585 ± 0.0007	−15.10 ± 0.76
GC030-33	1.0574 ± 0.0006	−15.50 ± 0.61	GC030-42	1.0553 ± 0.0008	−18.08 ± 0.85
GC030-34	1.0601 ± 0.0007	−13.05 ± 0.65	GC030-43	1.0556 ± 0.0008	−17.88 ± 0.87
GC030-35	1.0571 ± 0.0008	−15.86 ± 0.76	GC030-44	1.0561 ± 0.0008	−17.44 ± 0.86
GC030-36	1.0551 ± 0.0007	−17.86 ± 0.68			

(*Contd. overleaf*)

TABLE 1. (*contd.*) C analyses

Analysis label	$^{13}C/^{12}C \pm 1$ s ($\times 10^{-2}$)	$\delta^{13}C \pm 1$ s (‰PDB)	Analysis label	$^{13}C/^{12}C \pm 1$ s ($\times 10^{-2}$)	$\delta^{13}C \pm 1$ s (‰PDB)
22–23 August 1995 Standard regression line 3c3			Δ initial $= -45.01$‰	Δ final $= -45.56$‰	
GC030-45	1.0545 ± 0.0007	-16.26 ± 0.81	GC008-25	1.0630 ± 0.0007	-8.04 ± 0.70
GC030-46	1.0571 ± 0.0008	-13.79 ± 0.85	GC008-26	1.0630 ± 0.0008	-8.00 ± 0.75
GC030-47	1.0581 ± 0.0006	-12.88 ± 0.70	GC008-27	1.0618 ± 0.0006	-9.11 ± 0.64
GC030-48	1.0584 ± 0.0008	-12.57 ± 0.83	GC008-28	1.0600 ± 0.0007	-10.85 ± 0.66
GC030-49	1.0542 ± 0.0008	-16.43 ± 0.85	GC008-29	1.0631 ± 0.0007	-7.90 ± 0.73
GC030-50	1.0532 ± 0.0009	-17.38 ± 0.93	GC008-30	1.0641 ± 0.0007	-6.90 ± 0.73
GC008-18	1.0584 ± 0.0007	-12.49 ± 0.72	GC008-31	1.0627 ± 0.0007	-8.18 ± 0.67
GC008-19	1.0565 ± 0.0006	-14.28 ± 0.68	GC008-32	1.0588 ± 0.0007	-11.86 ± 0.72
GC008-20	1.0630 ± 0.0008	-8.20 ± 0.79	GC008-33	1.0578 ± 0.000	-12.72 ± 0.76
GC008-21	1.0628 ± 0.0007	-8.32 ± 0.70	GC008-34	1.0617 ± 0.000	-9.12 ± 0.73
GC008-22	1.0635 ± 0.0006	-7.69 ± 0.66	GC008-35	1.0577 ± 0.000	-12.78 ± 0.74
GC008-23	1.0591 ± 0.0007	-11.76 ± 0.75	GC008-36	1.0584 ± 0.0008	-12.14 ± 0.80
GC008-24	1.0582 ± 0.0008	-12.56 ± 0.75			

1. Analyses are listed in chronological order and divided into separate sessions, each calibrated against a different regression line.

2. Tabulated $^{12}C^{14}N/^{13}C$ and $^{13}C/^{12}C$ ratios are mean values calculated from multiple measurements made at each analysis point (50 individual measurements for N analyses and 100 for C). These measurements were corrected for dead-time of the counting system and any outliers more than $\pm 3\,S_x$ away from the mean value were rejected (where S_x is the standard deviation about the mean value).

3. The uncertainty in the mean value of $^{12}C^{14}N/^{13}C$ or $^{13}C/^{12}C$ is given by the standard error of the mean $S_{\bar{x}}$, calculated as $S_x/\sqrt{n}$ where n is the number of measurements used to calculate the mean value (see Fitzsimons *et al.*, in press).

4. Nitrogen contents (in ppm) for each analysis point on the sample are calculated from the mean $^{12}C^{14}N/^{13}C$ ratio by calibration against standard analyses made during the same analytical session, using the relationship:

$$N_{sample}\,(ppm) = N_{standard}\,(ppm) \times (^{12}C^{14}N/^{13}C_{sample})/(^{12}C^{14}N/^{13}C_{standard})$$

where $N_{standard}$ (ppm) is 230.4 ppm as measured by conventional combustion techniques, and $^{12}C^{14}N/^{13}C_{standard}$ at the time of the sample analysis is taken from the regression line for the standard analyses made in that session (Fig. 2). Note that all ppm values quoted here are ppm by weight, and can be converted into atomic ppm by multiplying by a factor of 0.8572.

5. The C isotope data are expressed in the conventional per mil $\delta^{13}C$ notation relative to the V-PDB standard. $\delta^{13}C$ values for each analysis point on the sample are calculated from the mean $^{13}C/^{12}C$ ratio by calibration against standard analyses made during the same analytical session. This corrects the isotope ratio for instrumental mass fractionation using the relationship:

$$\delta^{13}C_{sample} = [(\delta^{13}C_{standard}+1000) \times (^{13}C/^{12}C_{sample})/(^{13}C/^{12}C_{standard})]-1000$$

(Equation 35 of Fitzsimons *et al.*, in press) where $\delta^{13}C_{standard}$ is -23.92‰ as measured by conventional combustion techniques, and $^{13}C/^{12}C_{standard}$ at the time of the sample analysis is taken from the regression line for the standard analyses made in that session (Fig. 3).

6. The uncertainty in N content or $\delta^{13}C$ combines the uncertainty in both the sample isotope ratio (see 3 above) and the standard isotope ratio. The latter is calculated as the standard error of a predicted value from a regression line (Equation 36 of Fitzsimons *et al.*, in press). We have ignored the small uncertainties associated with the assumed standard composition and the dead-time correction.

7. The regression lines are labelled according to Figs 2 and 3 (e.g. line 2b1 is the first line in Fig. 2b etc.).

8. The magnitude of instrumental mass fractionation (Δ) between ^{13}C and ^{12}C during a given C analysis is calculated as the difference in per mil between the $\delta^{13}C$ value for the standard derived using the $^{13}C/^{12}C$ ratio from the relevant point of the regression line and the 'true' $\delta^{13}C$ value of the standard measured by bulk combustion. The slopes of the regression lines through the standard isotope data indicate that Δ varies with time in a linear or near-linear fashion. The table gives initial and final Δ values for each analytical session.

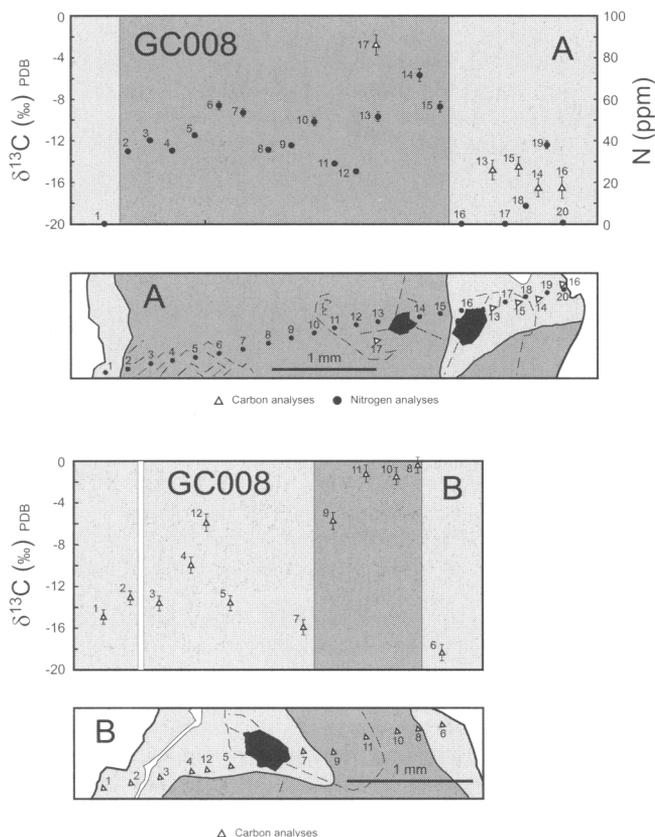FIG. 5. δ^{13}C and N (ppm) data for the four analytical transects (A, B [above], C and D [next page]) on plate GC008 (see Fig. 4 for their location). The top diagram for each transect presents analytical data (C data are open triangles, N data are filled circles) with ± 1 s error bars (in most cases the error bars for the N data are smaller than the symbol size). The horizontal axis in the top diagram represents distance, such that the position of the data points matches with the corresponding sputter pits in the bottom diagram, which illustrates the spatial distribution of the SIMS sputter pits relative to the diamond CL zones. The shading in both diagrams corresponds to the prominent CL zones in Fig. 4, and the symbol size reflects the size of the sputter pits on the sample surface.

higher N contents of 50–750 ppm. The C isotope data also show distinct correlations with CL. Typical δ^{13}C values for the central buff and the outer blue-green CL zones are −9 to 0‰ and −17 to −10‰ respectively, although some analyses near the boundary between the two suggest that either the sputter pits sampled both CL zones or the boundary is not as sharp in terms of δ^{13}C as it is in CL.

Plate GC030

Nitrogen and C data for this plate were collected from four analytical transects (Fig. 4), and the data are summarized in Fig. 6. The homogeneous yellow CL zone has N contents of 15–26 ppm, whereas the zoned blue-green CL zone exhibits an extreme variation, with very little N in the dark blue and green bands (<10 ppm) and relatively high N contents in the bright blue bands (typically 100–470 ppm). The δ^{13}C values vary between −20 and −11‰. There is extensive overlap in the C data from both CL zones, but the two data sets do have distinct distributions. The yellow zone (δ^{13}C = −20 to −15‰) tends to have lighter C isotope compositions than the blue-green zone (δ^{13}C = −18 to −11‰), and the former also has a smaller range of compositions.
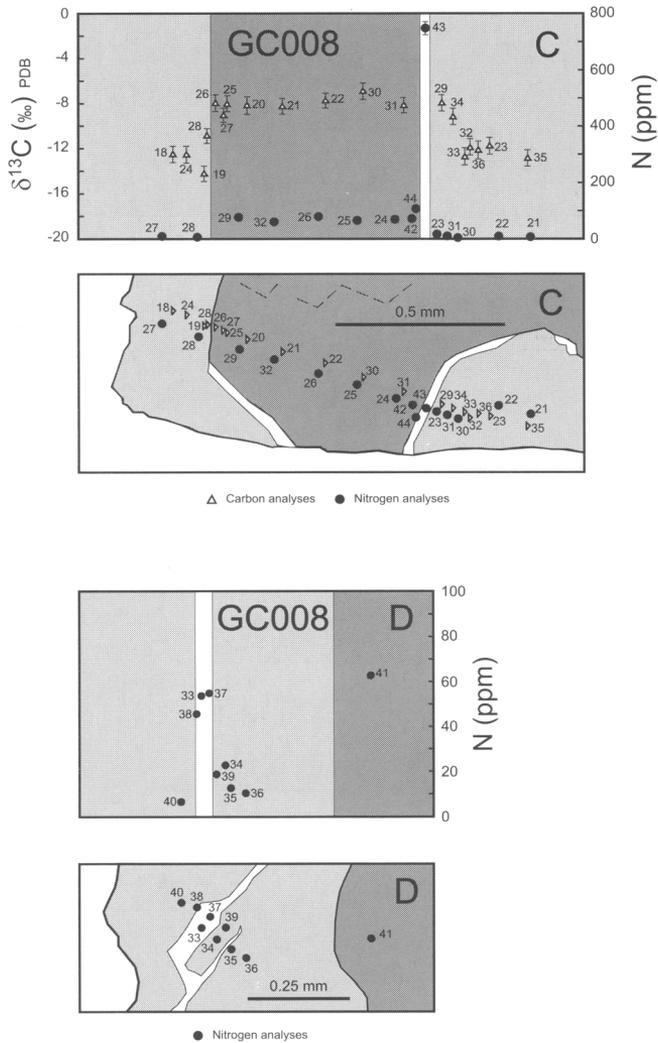
869

FIG. 5. (*contd.*)

Plate GC042

Nitrogen and C analyses of this plate followed a single transect (Fig. 4), and the data are summarized in Fig. 7. Nitrogen contents vary between 5 and 185 ppm. The transect does not cross any sharp CL boundaries, but the areas with high N content do correlate with brighter blue CL colours, whereas lower N contents correlate with less intense CL. The C isotope compositions vary between −8 and −1‰. There is no clear spatial pattern to the C isotope compositions, but the range is larger than the analytical uncertainty.

Summary and correlations between plates

Two distinct generations of diamond growth have been identified in the George Creek stones using CL characteristics (Chinn, 1995); homogeneous diamond with yellow-buff CL, and diamond with blue-green CL and complex growth patterns which in many cases are partly masked by slip planes. The microanalytical data presented here for three of the George Creek stones indicate that these two major growth generations are distinguished not only by their CL patterns, but also by their N contents and C isotope characteristics.
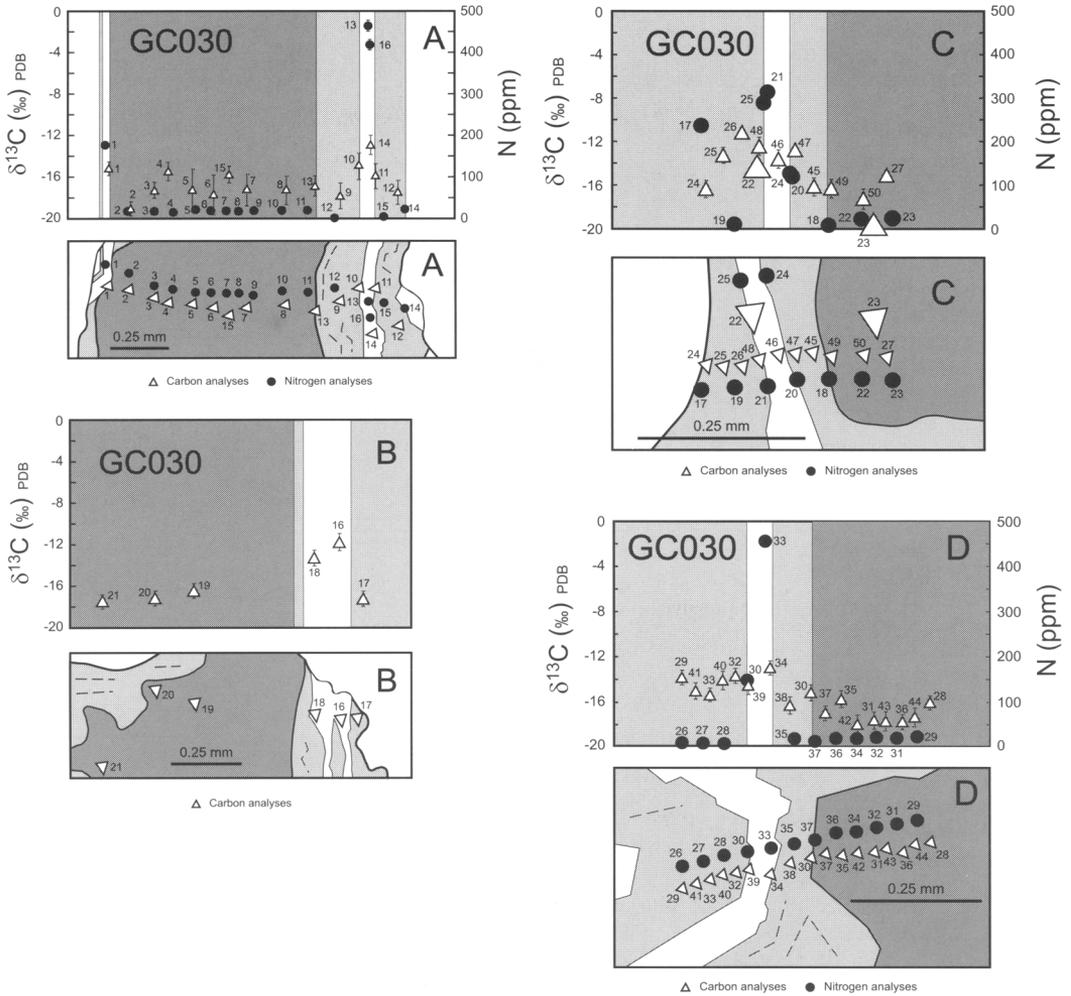
FIG. 6. $\delta^{13}C$ and N (ppm) data for the four analytical transects (A, B, C and D) on plate GC030 (see Fig. 4 for their location). Details as for Fig. 5. There are two symbol sizes for C analyses in transect C because the analyses were made in two sessions with different sizes of sputter pit.

Nitrogen contents show a consistent relationship with CL characteristics in all three stones. The homogeneous yellow-buff diamond generation has relatively low and homogeneous N content, whereas the blue-green diamond generation has a large variation in N content (Fig. 8), which correlates directly with CL intensity. Bright blue CL is associated with high N content (typically 50−750 ppm) whereas darker blue or green bands have very low N content (<20 ppm). These small-scale (~50 μm or less) spatial variations in the N content of blue-green diamond are particularly well preserved in plate GC030, where they clearly correlate with the complex oscillatory CL zonation. Significant N zonation is also preserved in the blue-green diamond of plates GC008 and GC042 even though growth features are largely obscured by intense slip plane development. Discontinuities in N content between different growth zones are sharp, although intermediate N contents were measured for sputter pits located on CL
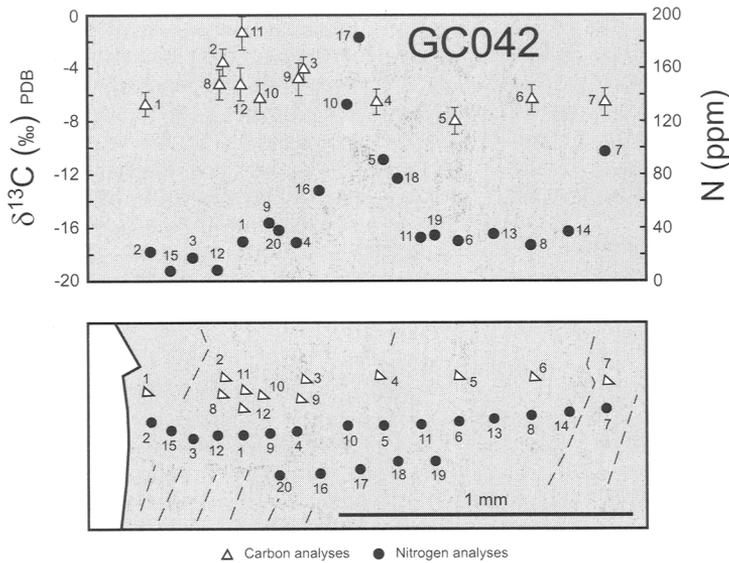
FIG. 7. $\delta^{13}C$ and N (ppm) data for the analytical transect on plate GC042 (see Fig. 4 for its location). Details as for Fig. 5.

boundaries, which presumably sampled more than one growth zone.

The SIMS N data are broadly consistent with the IR spectral measurements (Chinn, 1995), but the relatively large volume sampled for each IR spectrum obscures the chemical variation revealed by SIMS. The IR spectrometry is a transmission technique that collects data from a cylindrical sample volume with a depth equivalent to the plate thickness. In this case, the IR sample volume had a diameter of 80 μm and a depth of 0.5–1.6 mm depending on the plate, whereas each SIMS analysis sampled material from a cylinder with a diameter of 8 μm and a depth of 5 μm, corresponding to a volume at least four orders of magnitude smaller than that for the IR technique. The IR spectrometry is unsuitable for N analysis in diamonds like the George Creek stones, which have a growth zonation on a scale of less than 50 μm, and this has important implications for the determination of diamond thermal histories on the basis of N aggregation state.

Nitrogen aggregation state depends on the N concentration as well as the temperature–time history. For the same temperature–time history, diamond with a high N content is more likely to have highly aggregated N than diamond with a low N content, since the migration distances

required for N aggregation are smaller. The blue-green CL zones effectively comprise interlayered N-bearing (type I) and N-absent (type II) diamond. Although the percentage of B aggregates determined from an IR spectrum of interlayered type I and II diamond will be correct, most of the N is contained within only part of the analysed volume, and the N content of this type I diamond will be higher than that determined for the spectrum as a whole. This means that for an assumed mantle residence time, the calculated temperature will be an over-estimate, and this could account for the apparent 100°C discrepancy between the temperatures calculated for the George Creek stones from N aggregation state and those calculated from mineral inclusion thermobarometry.

George Creek diamonds also exhibit complex variations in C isotope composition (Fig. 9), and, although not as extreme as the variations in N content, they are significantly greater than any analytical uncertainty and are large compared with the range of $\delta^{13}C$ values commonly reported for bulk diamond analyses (Fig. 10). Indeed, the range of $\delta^{13}C$ values preserved by plate GC008 alone is greater than the range of values reported for entire diamond suites from many kimberlite pipes (e.g. Deines *et al.*, 1987, 1989, 1991). It is
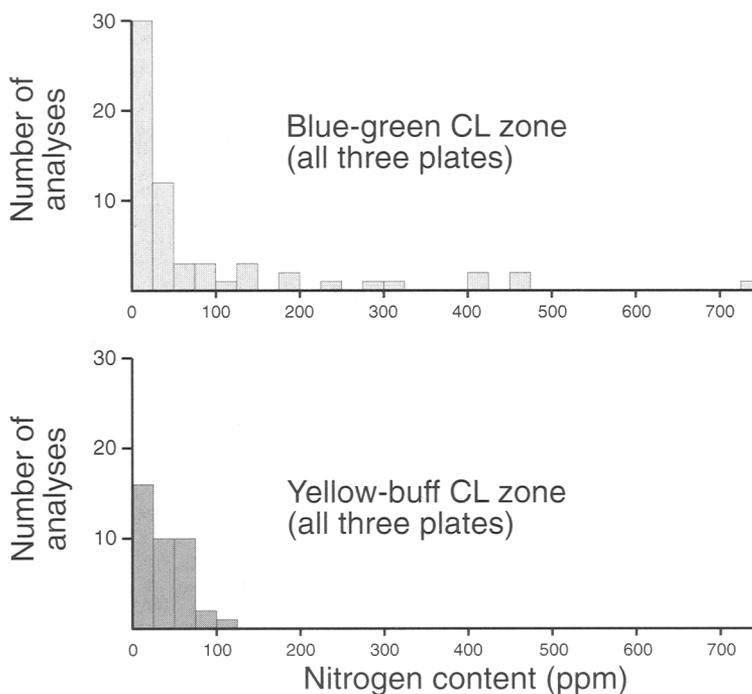
FIG. 8. Histograms for all of the N data collected from the George Creek plates, divided according to the two principal diamond generations. Diamond with homogeneous yellow-buff CL has a restricted range of low to moderate N contents (0–100 ppm), whereas diamond with zoned blue-green CL has very heterogeneous N contents. Most of the blue-green diamond (corresponding to the green or dark blue CL zones) has a very low N content (0–25 ppm) but the bright blue CL zones have high N contents (up to 750 ppm).

also notable that if the data for all three plates are combined, both of the major diamond generations exhibit a wide range in $\delta^{13}C$ values (Fig. 9). A number of conventional C isotope analyses of diamonds from George Creek (by gas-source mass spectrometry at the Open University, UK) have identified a $\delta^{13}C$ range of −28.5 to −15.6‰ for blue-green diamond and −31.0 to −8.0‰ for yellow-buff diamond (J. M. Gibson, pers. comm.), indicating that the C isotope variation within the George Creek suite as a whole is even wider than that revealed by the SIMS data presented here.

The wide range of $\delta^{13}C$ within plates GC008 and GC030 is in stark contrast to the SIMS data collected in a companion study of some Kaapvaal diamonds (Harte et al., 1999). These Kaapvaal diamonds have relatively homogeneous $\delta^{13}C$ values, and Harte et al. (1999) argue that this could reflect significant C diffusion during mantle residence. Distinct $\delta^{13}C$ distributions for the yellow-buff and blue-green diamond in both

GC008 and GC030 (Fig. 9) imply that any C diffusion in the George Creek diamonds has been on a very limited scale.

Unlike the direct correlation between N and CL characteristics, there is no consistent relationship between CL and $\delta^{13}C$ (Figs 9, 11). The homogeneous yellow-buff diamond in plate GC008 ($\delta^{13}C$ = −9 to 0‰) has a quite distinct C isotope composition from that in plate GC030 ($\delta^{13}C$ = −20 to −15‰). Similarly, the C isotope composition of the blue-green diamond varies from stone to stone (Fig. 11). Blue-green diamond in plates GC008 and GC030 has relatively light C isotope compositions ($\delta^{13}C$ = −17 to −6‰ and −18 to −11‰ respectively) whereas plate GC042, which is composed entirely of blue-green diamond, has relatively heavy C isotope compositions ($\delta^{13}C$ = −8 to −1‰).

There is also evidence for isotopic variation within the major diamond generations. The spread of $\delta^{13}C$ values in the blue-green diamond is
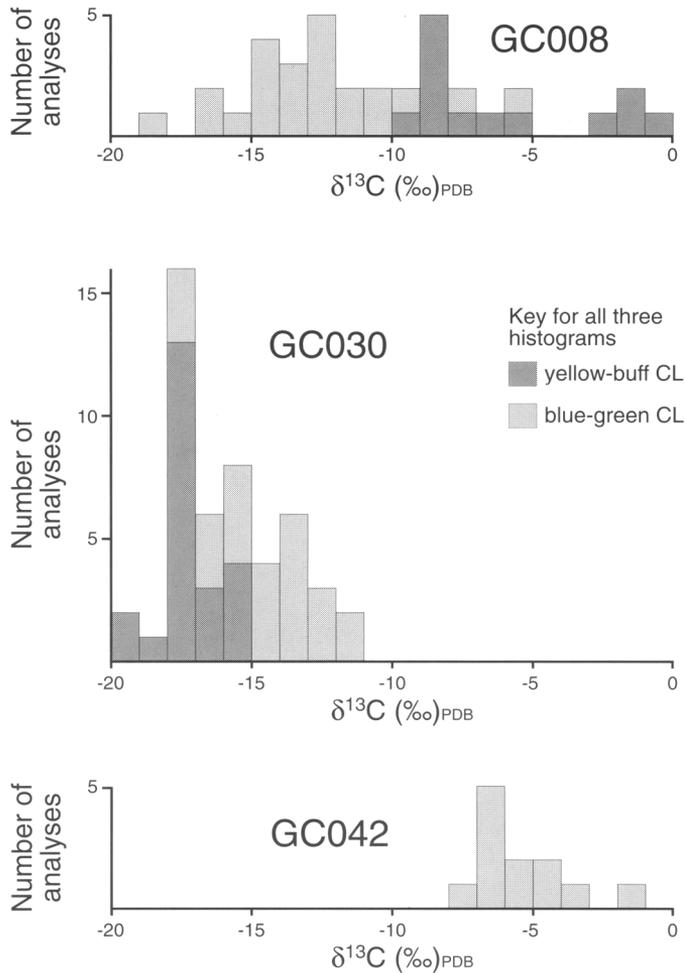
FIG. 9. Histograms for all of the C data collected from the George Creek plates, depicting the ranges in isotope composition for the yellow-buff and blue-green diamond in each stone. Given an uncertainty (at the 1 s level) of ±0.5 to 1.2‰ for the C isotope analyses, a distribution encompassing a range of 2 to 5‰ could be due solely to analytical error (i.e. ±2 s), but both GC008 and GC030 are clearly composed of two diamond generations with distinct isotope compositions, corresponding to the two major CL zones in each stone. It is also apparent that diamond generations in different stones but with the same CL characteristics do not necessarily have the same C isotope composition.

greater than analytical uncertainty in all three plates. The C data from transects A and B in plate GC030 suggest that the N-rich bright blue CL zones have a heavier C isotopic composition than the dark blue and green zones, but there is no obvious correlation between $\delta^{13}C$ and CL colour or N content in the other transects across this stone or in the data from GC008 and GC042. The yellow-buff diamond has a smaller range of $\delta^{13}C$

values than coexisting blue-green diamond in plates GC008 and GC030, although the −9 to 0‰ $\delta^{13}C$ range in the yellow-buff diamond of plate GC008 is still greater than analytical uncertainty and indicates that this diamond generation also preserves an isotopic heterogeneity, albeit smaller than that in the blue-green diamond.

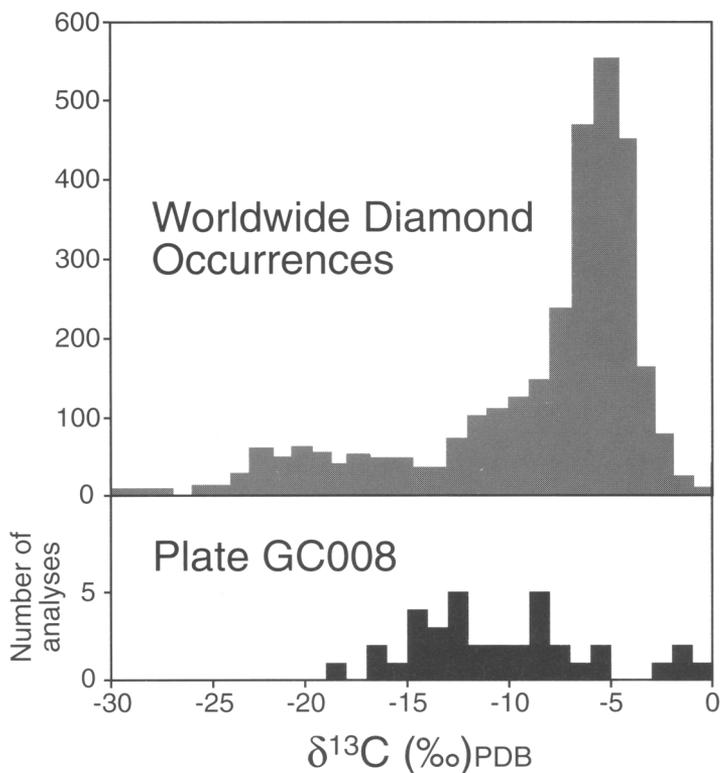Overall, this study confirms the exceptional nature of the yellow-buff CO_2-bearing diamond

FIG. 10. A comparison of $\delta^{13}C$ values for the 36 SIMS analyses of plate GC008 (this study) with $\delta^{13}C$ values for worldwide diamond occurrences (compiled by van Heerden *et al.*, 1995, from 2946 diamond analyses reported in the literature).

(Chinn, 1995), whereas the blue-green diamond is similar to diamond found elsewhere. Small-scale growth zones distinguished by their blue-green CL colours are a relatively common feature of natural diamond, and the data presented here (and by Harte *et al.*, 1999) indicate that such zones are defined by marked oscillations in N content. These oscillations are presumably controlled by fluctuations in the composition of the local fluid reservoir during diamond growth, although the potential role of growth kinetics (i.e. differences in growth rate and mechanism) in determining N content cannot be discounted (e.g. Lang, 1974; Boyd *et al.*, 1988; Kanda and Yamaoka, 1993; Cartigny *et al.*, 1997). Variations in $\delta^{13}C$ are less obvious within these oscillatory growth zones, and there is no clear evidence in the George Creek data for significant fractionation of C isotopes between crystallizing diamond and a fluid reservoir (Deines, 1980) despite the evidence for

large fluctuations in N content. Large variations in C isotope composition occurred between distinct generations of diamond growth rather than during relatively short-term fluctuations or during a single growth period, and these variations do not correlate in any consistent way with other diamond characteristics, suggesting that $\delta^{13}C$ was independent of the growth process. It seems likely that the extreme variations in $\delta^{13}C$ reported here reflect temporal and/or spatial compositional variations in the mantle fluid reservoir, which were controlled externally by pre-existing isotopic heterogeneities rather than by the process of diamond precipitation. The chemical variations revealed by SIMS analysis of the George Creek stones are consistent with a complicated history of diamond growth under a variety of physical and chemical conditions, as is being increasingly recognized in other diamond suites (e.g. Bulanova, 1995; Deines *et al.*, 1997).

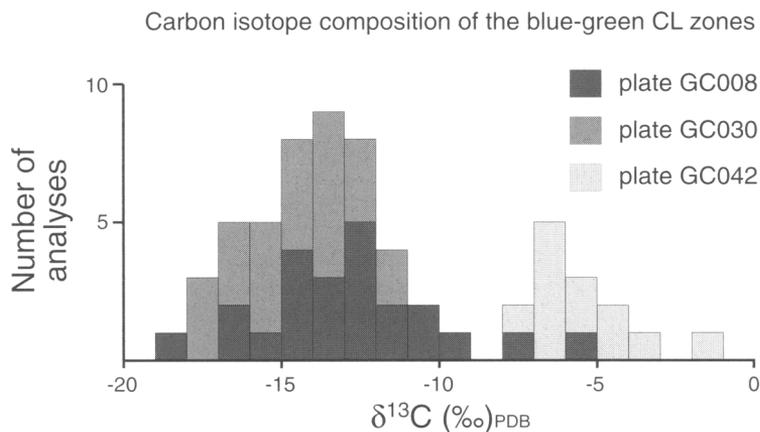Carbon isotope composition of the blue-green CL zones

FIG. 11. A histogram of all the C analyses made of the blue-green diamond generation in the three George Creek plates. This diamond generation has a different distribution of $\delta^{13}C$ values in each of the three plates.

Conclusions

The ion probe data described above have a number of important implications, although the remarkable relationships preserved by these unusual stones from George Creek need not be typical of relationships elsewhere. (1) Individual diamonds from George Creek preserve a wide range of N contents and of C isotope compositions, which are similar to the compositional ranges identified within entire diamond suites from many kimberlite pipes (e.g. Deines *et al.*, 1987, 1989, 1991). (2) Complex CL patterns within individual stones from George Creek reveal two types of heterogeneity: (a) two major generations of diamond growth, one with homogeneous yellow-buff CL and the other with zoned blue-green CL, and (b) growth zonation on a 10–50 μm scale within the blue-green diamond. (3) Nitrogen content correlates directly with CL colour and intensity. Diamond with homogeneous yellow-buff CL has uniform N contents, whereas diamond with zoned blue-green CL has variable N contents. On a smaller scale, bright blue CL zones in the blue-green diamond are N rich (type-I diamond), whereas less-intense dark blue or green CL zones are N poor (type-II diamond). In general, bright CL zones have a high N content and dark CL zones have a low N content. (4) C isotope composition also varies between the two diamond growth generations, but not in a consistent manner. The homogeneous yellow-buff diamond has a lighter isotope composition than the zoned blue-green diamond in some stones, whereas in others the yellow-buff diamond has a heavier isotope composition than the blue-green diamond. (5) There is also a variation in C isotope composition within the major growth generations. The variation in the zoned blue-green diamond has a greater magnitude than that in the homogeneous yellow-buff diamond, but again there is no consistent relationship between $\delta^{13}C$ and CL colour or N content. (6) The CL characteristics are a good measure of the homogeneity and relative concentration of N in diamond, both within individual stones and between different stones. In contrast, CL is a poor guide to areas of varying C isotope composition. (7) SIMS is a valuable technique for the quantification of N zonation in diamond, which can occur on a scale comparable to the sample volume of a single SIMS analysis. In contrast, IR spectroscopy is a transmission technique that typically analyses a sample volume which is at least four orders of magnitude greater than that used in SIMS, and as such is not suitable for isolating individual growth zones. The IR technique will only provide an average N concentration for diamond with zonation on the scale exhibited by the George Creek stones. These average data can lead to erroneous conclusions when used to infer diamond thermal histories from N aggregation state, and IR data should be interpreted with care in cases where micron-scale N zonation is suspected. (8) The George Creek stones preserve evidence of temporal and/or spatial variations in the C isotope composition

and N content of mantle fluids during diamond growth. The N zonation within the blue-green diamond indicates substantial oscillatory fluctuations in the uptake of N into diamond over a relatively short time scale, which could reflect open-system compositional changes in the local fluid reservoir, or a variation in the diamond growth rate. The magnitude of these fluctuations is greater than the differences in N content between the two major growth generations. In contrast, the differences in $\delta^{13}C$ between the major growth generations are more significant than those within them. These isotopic variations are likely to reflect pre-existing heterogeneities in mantle fluids and there is no evidence for significant C isotope fractionation during precipitation of the George Creek diamonds. (9) The lack of any consistent correlation between the N and C data implies that the factors controlling the incorporation of N during diamond growth do not directly control $\delta^{13}C$.

Acknowledgements

References

Bennett, V.C. and DePaolo, D.J. (1987) Proterozoic crustal history of the western United States as determined by neodymium isotopic mapping. *Geol. Soc. Am. Bull.*, **99**, 674–85.

Bertrand, P. and Mercier, J.-C.C. (1985) The mutual solubility of coexisting ortho- and clinopyroxene: toward an absolute geothermometer for the natural system? *Earth Planet. Sci. Lett.*, **76**, 109–22.

Boyd, S.R. and Pillinger, C.T. (1994) A preliminary study of $^{15}N/^{14}N$ in octahedral growth form diamonds. *Chem. Geol.*, **116**, 43–59.

Boyd, S.R., Mattey, D.P., Pillinger, C.T., Milledge, H.J., Mendelssohn, M. and Seal, M. (1987) Multiple growth events during diamond genesis: an integrated study of carbon and nitrogen isotopes and nitrogen aggregation state in coated stones. *Earth Planet. Sci. Lett.*, **86**, 341–53.

Boyd, S.R., Pillinger, C.T., Milledge, H.J., Mendelssohn, M.J. and Seal, M. (1988) Fractionation of nitrogen isotopes in a synthetic diamond of mixed crystal habit. *Nature*, **331**, 604–7.

Boyd, S.R., Pillinger, C.T., Milledge, H.J., Mendelssohn, M.J. and Seal, M. (1992) C and N isotopic composition and the infrared absorption spectra of coated diamonds: evidence for the regional uniformity of CO_2-H_2O rich fluids in lithospheric mantle. *Earth Planet. Sci. Lett.*, **109**, 633–44.

Boyd, S.R., Pineau, F. and Javoy, M. (1994) Modelling the growth of natural diamonds. *Chem. Geol.*, **116**, 29–42.

Bulanova, G.P. (1995) The formation of diamond. *J. Geochem. Explor.*, **53**, 1–23.

Cartigny, P., Boyd, S.R., Harris, J.W. and Javoy, M. (1997) Nitrogen isotopes in peridotitic diamonds from Fuxian, China: the mantle signature. *Terra Nova*, **9**, 175–179.

Chinn, I.L. (1995) *A study of unusual diamonds from the George Creek K1 kimberlite dyke, Colorado*. Ph.D. thesis (unpubl.), University of Cape Town.

Deines, P. (1980) The carbon isotopic composition of diamonds: relationship to diamond shape, color, occurrence and vapor composition. *Geochim. Cosmochim. Acta*, **44**, 943–61.

Deines, P., Gurney, J.J. and Harris, J.W. (1984) Associated chemical and carbon isotopic composition variations in diamonds from Finsch and Premier kimberlite, South Africa. *Geochim. Cosmochim. Acta*, **48**, 325–42.

Deines, P., Harris, J.W. and Gurney, J.J. (1987) Carbon isotopic composition, nitrogen content and inclusion composition of diamonds from the Roberts Victor kimberlite, South Africa: evidence for ^{13}C depletion in the mantle. *Geochim. Cosmochim. Acta*, **51**, 1227–43.

Deines, P., Harris, J.W., Spear, P.M. and Gurney, J.J. (1989) Nitrogen and ^{13}C content of Finsch and Premier diamonds and their implications. *Geochim. Cosmochim. Acta*, **53**, 1367–78.

Deines, P., Harris, J.W. and Gurney, J.J. (1991) The carbon isotopic composition and nitrogen content of lithospheric and asthenospheric diamonds from the Jagersfontein and Koffiefontein kimberlite, South Africa. *Geochim. Cosmochim. Acta*, **55**, 2615–25.

Deines, P., Harris, J.W. and Gurney, J.J. (1997) Carbon isotope ratios, nitrogen content and aggregation state, and inclusion chemistry of diamonds from Jwaneng, Botswana. *Geochim. Cosmochim. Acta*, **61**, 3993–4005.

Eggler, D.H., Meen, J.K., Welt, F., Dudas, F.O., Furlong, K.P., McCallum, M.E. and Carlson, R.W. (1988) Tectonomagmatism of the Wyoming Province. *Colo. Sch. Mines Q.*, **83**, 25–40.

Eiler, J.M., Valley, J.W., Graham, C.M. and Baumgartner, L.P. (1995) Ion microprobe evidence for the mechanisms of stable isotope retrogression in high-grade metamorphic rocks. *Contrib. Mineral. Petrol.*, **118**, 365–78.

Ellis, D.J. and Green, D.H. (1979) An experimental study of the effect of Ca upon garnet-clinopyroxene Fe-Mg exchange equilibria. *Contrib. Miner. Petrol.*, **71**, 13–22.

Evans, T. (1992) Aggregation of nitrogen in diamond. In *The properties of natural and synthetic diamond* (J.E. Field, ed.). Academic Press, London, pp. 259–90.

Evans, T. and Harris, J.W. (1989) Nitrogen aggregation, inclusion equilibration temperatures and the age of diamonds. In *Kimberlites and related rocks, vol. 2* (J. Ross, ed.). Geological Society of Australia, Spec. Publ., **14**, Blackwell Scientific, Melbourne, pp. 1001–6.

Fitzsimons, I.C.W., Harte, B. and Clark, R.M. (in press) SIMS stable isotope measurement: counting statistics and analytical precision. *Mineral. Mag.*

Galimov, E.M. (1991) Isotope fractionation related to kimberlite magmatism and diamond formation. *Geochim. Cosmochim. Acta*, **55**, 1697–708.

Harris, J.W. (1987) Recent physical, chemical, and isotopic research of diamond. In *Mantle xenoliths* (P.H. Nixon, ed.). John Wiley & Sons, Chichester, pp. 477–500.

Harte, B. and Otter, M. (1992) Carbon isotope measurements on diamonds. *Chem. Geol.*, **101**, 177–83.

Harte, B., Fitzsimons, I.C.W., Harris, J.W. and Otter, M.L. (1999) Carbon isotope ratios and nitrogen abundances in relation to cathodoluminescence characteristics for some diamonds from the Kaapvaal Province, S. Africa. *Mineral. Mag.*, **63**, 829–56.

Helmstaedt, H.H. and Gurney, J.J. (1995) Geotectonic controls of primary diamond deposits: implications for area selection. *J. Geochem. Explor.*, **53**, 125–44.

Hoffman, P.F. (1990) Geological constraints on the origin of the mantle beneath the Canadian shield. *Phil. Trans. R. Soc. London*, **A331**, 523–32.

Javoy, M., Pineau, F. and Demaiffe, D. (1984) Nitrogen and carbon isotopic composition in the diamonds of Mbuji Mayi, Zaïre. *Earth Planet. Sci. Lett.*, **68**, 399–412.

Kanda, H. and Yamaoka, S. (1993) Inhomogeneous distribution of nitrogen impurities in {111} growth sectors of high pressure synthetic diamond. *Diamond and Related Materials*, **2**, 1420–3.

Karlstrom, K.E. and Houston, R.S. (1984) The Cheyenne Belt: analysis of a Proterozoic suture in southern Wyoming. *Precambrian Res.*, **25**, 415–46.

Kirkley, M.B., Gurney, J.J., Otter, M.L., Hill, S.J. and Daniels, L.R. (1991) The application of C isotope measurements to the identification of the sources of C in diamonds: a review. *Appl. Geochem.*, **6**, 477–94.

Lang, A.R. (1974) On the growth-sectorial dependence of defects in natural diamonds. *Proc. R. Soc. London*, **A340**, 233–48.

Nickel, K.G. and Green, D.H. (1985) Empirical geothermobarometry for garnet peridotites and implications for the nature of the lithosphere, kimberlites and diamonds. *Earth Planet. Sci. Lett.*, **73**, 158–70.

Reed, J.C., Ball, T.T., Farmer, G.L. and Hamilton, W.B. (1993) A broader view. In *The geology of North America, vol. C-2, Precambrian: Conterminous U.S.* (J.C. Reed, et al., eds.). Geological Society of America, Boulder, Colorado, pp. 597–636.

Slodzian, G. (1980) Microanalyzers using secondary ion emission. *Adv. Electronics Electron Phys. Suppl.*, **13B**, 1–44.

Smith, M.P. and Yardley, B.W.D. (1996) The boron isotopic composition of tourmaline as a guide to fluid processes in the southwestern England orefield: an ion microprobe study. *Geochim. Cosmochim. Acta*, **60**, 1415–27.

Swart, P.K., Pillinger, C.T., Milledge, H.J. and Seal, M. (1983) Carbon isotopic variation within individual diamonds. *Nature*, **303**, 793–5.

Taylor, W.R., Jaques, A.L. and Ridd, M. (1990) Nitrogen-defect aggregation characteristics of some Australasian diamonds: time-temperature constraints on the source regions of pipe and alluvial diamonds. *Amer. Mineral.*, **75**, 1290–310.

Taylor, W.R., Canil, D. and Milledge, H.J. (1996) Kinetics of Ib to IaA nitrogen aggregation in diamond. *Geochim. Cosmochim. Acta*, **60**, 4725–33.

Valley, J.W. and Graham, C.M. (1991) Ion microprobe analysis of oxygen isotope ratios in granulite facies magnetites: diffusive exchange as a guide to cooling history. *Contrib. Mineral. Petrol.*, **109**, 38–52.

van Heerden, L.A., Gurney, J.J. and Deines, P. (1995) The carbon isotopic composition of harzburgitic, lherzolitic, websteritic and eclogitic paragenesis diamonds from southern Africa: a comparison of genetic models. *S. Afr. J. Geol.*, **98**, 119–25.

Zinner, E., Ming, T. and Anders, E. (1989) Interstellar SiC in the Murchison and Murray meteorites: isotopic composition of Ne, Xe, Si, C and N. *Geochim. Cosmochim. Acta*, **53**, 3273–90.

Plate Captions

PLATE 1. Photograph of the polished 'wild-one' diamond plate (0.4 mm thick plate cut across centre of Bultfontein specimen J/1064.2). This colour photo shows the whole of the plate, with the major discontinuity representing a fracture across the plate; whilst Fig. 2a shows the upper part of the specimen on the side analysed, which is the opposite side of the diamond plate to that seen in above. The major zone labels (A, B, C, D, E) correspond with those of Fig. 2a, and comparison with Fig. 2a shows that although the same broad pattern of zones and subzones is seen on both sides of the diamond plate, there are definite differences in detail. The CL reveals spectacular growth zones of both cuboid and octahedral type. The areas with brighter, lighter blue colours have high N abundances; the very dark and yellow-green coloured subzones (labelled subzones C3, D3, E2 in Fig. 2a) are marked by low N abundances. The width of the plate is 3.3 mm.

PLATE 2. (a) Photograph of cut, polished and analysed surface of 'whopper' diamond (off-centre section of Bultfontein specimen J/1063.1) in CL. The interior of the diamond is dominated by a series of largely cuboid growth zones mainly showing high luminescence; whilst the external parts show more regular and planar octahedral growth zones. A narrow zone of virtually zero luminescence is seen as the discontinuous black zone (labelled zone B in Fig. 3) in the outer part of the dominantly cuboid area. The width of the polished section is 4.7 mm. (b) Photograph of cut, polished and analysed surface of Koffiefontein K3 diamond in CL; note that extensive regions at bottom and right of photograph are the rough sides of the diamond, with the margin of the polished surface being marked by a zone (D in Fig. 5) of thin growth lines of variable CL. This diamond shows 'seeds' of rectilinear (octahedral) shape, towards right side of polished surface and marked by dominantly pale/bright blue CL colours. The 'seeds' may join outside the plane of the section and are surrounded by a zone (C of Fig. 5) of fairly uniform dark CL. The maximum width of the polished surface is 2.3 mm.

PLATE 3. Cathodoluminescence photographs of George Creek diamond plates. In all cases the dominant features are illustrated more clearly in the schematic diagrams of Fig. 4. (a) Plate GC008. The surface of this composite diamond comprises a central region with homogeneous buff CL, and outer areas dominated by dark green CL, with bright blue CL growth zones and yellow-green slip planes. The CL features around the dark mineral inclusions are largely obscured by bright patches produced by curving cracks beneath the plate surface. Plate dimensions are 5 mm × 4 mm, and linear trails of SIMS sputter pits are just visible crossing the plate surface. (b) Plate GC030. This composite diamond comprises a central region with yellow CL, and outer areas with blue-green CL and a complex growth zonation. Plate dimensions are 4 mm × 2 mm, and SIMS sputter pits are clearly visible on the plate surface. (c) Plate GC042. This diamond has blue-green CL, and is cut by thin yellowish slip planes in three principal orientations. Plate dimensions are 3 mm × 2 mm, and SIMS sputter pits are clearly visible on the plate surface crossing areas of blue and green CL.